AGU PUBLICATIONS

JGR

Journal of Geophysical Research: Solid Earth

RESEARCH ARTICLE
10.1002/2016JB013715

Key Points:
- Seismicity rates show 20 year long trends after removal of aftershocks in the northern Japanese subduction zone
- These trends are consistent with known changes in seismic coupling, with a better spatial resolution
- Regional postseismic quiescence is observed in the north of the studied zone and progressive decoupling offshore the Kanto region

Supporting Information:
- Supporting Information S1

Correspondence to:
D. Marsan,
david.marsan@univ-smb.fr

Citation:
Marsan, D., M. Bouchon, B. Gardonio, H. Perfettini, A. Socquet, and B. Enescu (2017), Change in seismicity along the Japan trench, 1990–2011, and its relationship with seismic coupling, *J. Geophys. Res. Solid Earth*, *122*, doi:10.1002/2016JB013715.

Received 3 NOV 2016
Accepted 15 MAY 2017
Accepted article online 17 MAY 2017

Change in seismicity along the Japan trench, 1990–2011, and its relationship with seismic coupling

D. Marsan[1,2], M. Bouchon[2,3], B. Gardonio[1,2], H. Perfettini[3,4], A. Socquet[2,3], and B. Enescu[5]

[1]Université de Savoie Mont Blanc, ISTerre, Le Bourget du Lac, France, [2]CNRS, ISTerre, Le Bourget du Lac, France, [3]Université Grenoble Alpes, ISTerre, Grenoble, France, [4]IRD, ISTerre, Grenoble, France, [5]Department of Geophysics, Kyoto University, Kyoto, Japan

Abstract We investigate the temporal evolution of the background seismicity rate related to the subduction of the Pacific plate in northeast Japan, at latitudes 34° to 42°, for the 1 January 1990 to 9 March 2011 period. Two declustering methods are used to identify robust features. We find that the dominant behavior is a lowering down of activity, especially in the northern half of our studied area, where changes appear related to the cycle of *M*7.5+ earthquakes, in particular the 1968 Tokachi and the 1994 Sanriku earthquakes. Acceleration of background seismicity is observed offshore the Kanto region and could mark a long-term decoupling of the Pacific and the Philippine Sea plates over a 100 km long segment along the Sagimi Trough, which cannot be simply explained by the earthquake cycle model. Our analysis further suggests that changes in background seismicity are plausibly related to changes in seismic coupling and thus further strengthens the recent observation that seismic coupling does vary at the timescales of tens of years, for the Japanese subduction zone.

1. Introduction

Recent observations have pointed out slow changes in slip deficit rates in the northern Japanese subduction zone, along the Japan trench. Far from being stable over years, the displacement of inland GPS stations shows consistent changes in rate between the 1996–2003 and the 2003–2011 periods [*Mavrommatis et al.*, 2014; *Yokota and Koketsu*, 2015]. These changes can be explained by (i) an increase in slip deficit rate offshore Iwate prefecture, coherent with the increase in coupling observed by Loveless and Meade (2016) in this zone over 1996–2011, and (ii) a decrease of geodetic coupling offshore central Tohoku. While (i) is likely related to previous large earthquakes, in particular the 1994 M_w7.6 Sanriku and the 2003 M_w8.1 Tokachi earthquakes (cf. Figure 1), (ii) is not, given its distance to these ruptures. The decoupling (ii) could have contributed to the occurrence of the 2011 M_w9.0 Tohoku earthquake that nucleated just updip.

The apparent strengthening of coupling offshore Iwate was already reported by *Ozawa et al.* [2007]. They attributed it to a cycle in coupling, i.e., a sudden decrease followed by a slow recovery, initiated by the 1994 Sanriku earthquake. The recovery extended well past the termination of the large afterslip triggered by the 1994 shock, which was effectively over by 1998 [*Heki*, 2007]. Arguing that the end of the afterslip in 1998 and the observed increase in coupling that started in 2003 are well separated in time, *Heki and Mitsui* [2013] instead proposed that the 2003 Tokachi earthquake caused the change in coupling offshore Iwate.

Time series of repeating earthquakes display rate changes in accordance with the GPS inversions of changes in slip deficit rates [*Mavrommatis et al.*, 2015], i.e., rates of repeaters increase when coupling decreases, although it is unclear how repeaters are potentially affected by local main shocks. More to the south, *Reverso et al.* [2016] observed a regular increase, over the 1990–2015 period, of the seismicity rate in the Boso area, known for its recurrent slow slip events (SSEs). They analyzed the seismicity close to the upper surface of the subducting Philippine Sea plate (PHS) in this area. After removing both short-lived transients, in particular related to SSEs, and aftershock activity, a 25 year long acceleration of so-called background activity can be isolated, that is well fitted by a constantly accelerating rate. This long-term acceleration is consistent with the shortening of recurrence times of the SSEs since 1996 [*Ozawa*, 2014]: the stressing rate of asperities (rupturing either as normal or as slow earthquakes) on the slip interface between PHS and the overriding Okhotsk plate (OKH) has been experiencing an increase over the last 25 years at least, akin to a slow uncoupling of this interface.

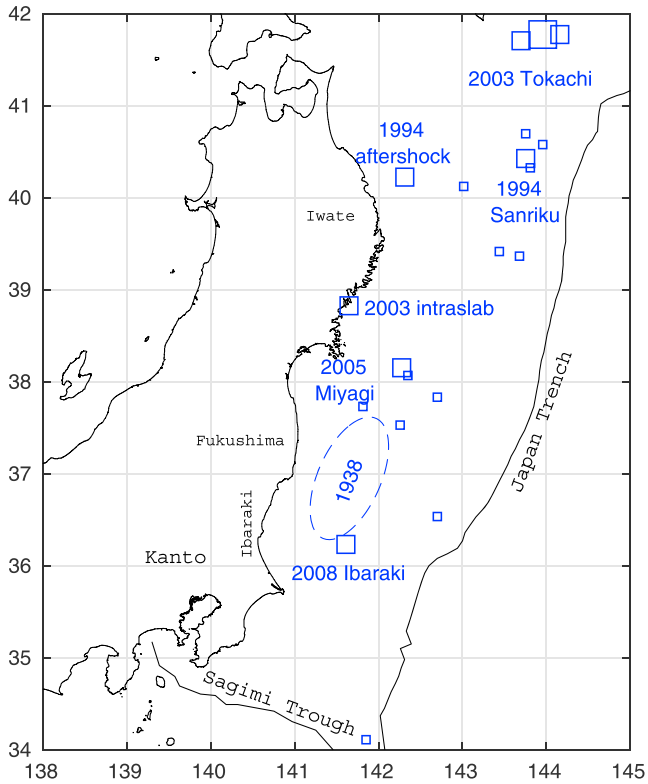

Figure 1. Map of the zone studied, with the 2003 Tokachi earthquake (the only *M*8 event here) shown with a big square, $8 > m \geq 7.0$ earthquakes with medium-sized squares and named. Smaller squares show $6.5 \leq m < 7.0$ earthquakes. The rupture area of the thrust 1938 sequence [*Abe*, 1977] is shown with dashed lines.

Why would this area undergo such an accelerated forcing remains unclear, although numerical simulations have shown that earthquake nucleation and the resulting slow stress concentration could cause the shortening of the SSE cycle [*Matsuzawa et al.*, 2010; *Mitsui*, 2015] and presumably the acceleration of seismicity as well.

We here study slow changes in background seismicity rates along the Japan trench, for the 1990–2011 period, and investigate how they are related to seismic coupling and its evolution. Earthquake activity is complementary to GPS observations for studying slow changes in slip deficit rate, by providing a longer historical record, and a more accurate localization, especially when considering the lack of resolution of GPS inversions near the trench or at depth. However, earthquake activity displays a natural variability and intermittency, mostly owing to clustering. This requires a prior processing of the seismicity rate in order to isolate long-term changes potentially hidden in the apparent complexity of this signal.

2. Data and Methods

We analyze the earthquakes listed in the Japan Meteorological Agency (JMA) seismological bulletins, with epicenters in the latitude 34°–42° and longitude 138°–145° area. We specifically focus on the 16551 $m \geq 3.0$ earthquakes occurring in the 1 January 1990 to 9 March 2011 period, which are within 20 km of the Pacific plate (PAC) interface as defined by *Hayes et al.* [2012], hence removing all crustal seismicity, as well as most earthquakes related to the subduction of PHS below and offshore the Kanto region, see Figure 2a. The selected earthquakes are thus ruptures occurring either on the upper surface of the slab, or within the slab. We stop our analysis at the time of the M_w7.3 foreshock of the 2011 *M*9.0 Tohoku earthquake, as this sequence strongly modified the seismic activity in the region. Removal of the numerous aftershocks of the *M*9.0 earthquake would require a specific treatment, facilitated by a longer observation time. The completeness magnitude for subduction earthquakes in this zone and time period is 2.6, so our data set selected at $m \geq 3.0$ is complete (cf. Figure 2b). The most notable earthquakes are the interplate Sanriku 18 July 1992 *M*6.9 doublet [*Kawasaki et al.*, 2001], the Sanriku 28 December 1994 *M*7.6 earthquake [*Yagi et al.*, 2003], the Tokachi 25 September 2003

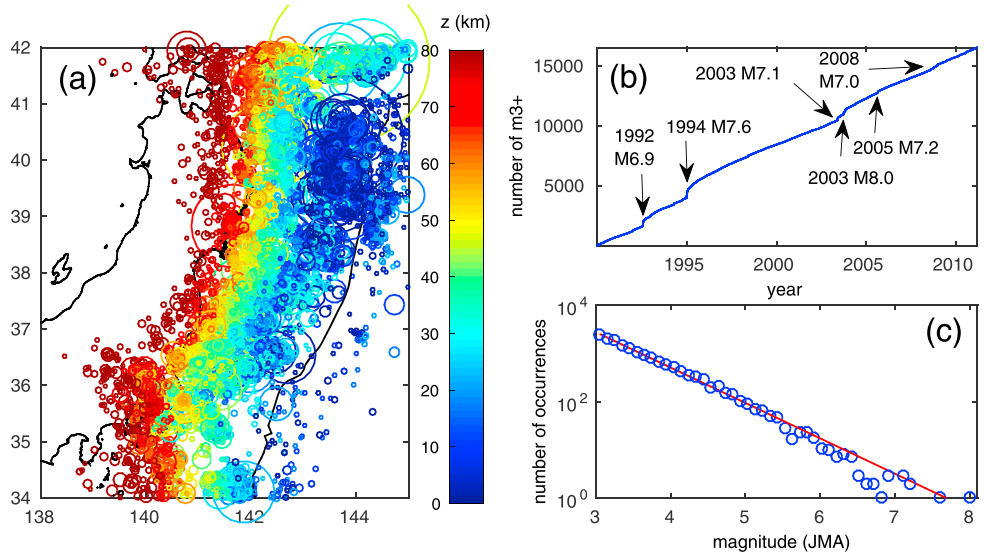

Figure 2. Earthquake data set analyzed, for the period 1 January 1990 to 9 March 2011. (a) Map of epicenters, color coded according to depth. (b) Time series of $m \geq 3$ earthquakes, with dates of the most notable shocks. (c) Occurrences versus JMA magnitudes, along with the best fit (in red) yielding a b value of 0.74. This relatively low value is consistent with the analysis of *Tormann et al.* [2015].

M_w8.1 earthquake, the Miyagi 16 August 2005 M7.2 earthquake, the Ibaraki 8 May 2008 M7.0 earthquake [*Kubo et al.*, 2013], and the 26 May 2003 M7.1 intraslab earthquake [*Okada and Hasegawa*, 2003], see Figures 1 and 2b. Occasionally, we perform additional analyses at a longer timescale, sometimes stretching as far back as 1923. Because depth is not well resolved, or even not resolved at all, for older earthquakes, we only use epicenter information for this longer catalog, i.e., we do not select earthquakes based on their proximity to the slab. The JMA data set is found to be complete for this area above magnitude 5.0 since 1923.

Similar to GPS displacements, earthquake time series must be processed to separate the different factors contributing to seismicity rate changes: stress changes generated coseismically by main shocks, stress changes due to postseismic relaxation (afterslip and viscous relaxation), and the background forcing. Both coseismic and postseismic triggering are here modeled as $1/t$ decaying contributions and are thus indistinguishable from one another in our approach. However, while transients in surface displacements are dominated by a few large main shocks, seismicity dynamics are affected by main shocks of all sizes [*Helmstetter*, 2003; *Marsan*, 2005], as clustering in space and time causes earthquake occurrences to be significantly dependent on previous events. Declustering amounts to such a removal of coseismic and postseismic effects, with the aim of reducing, if not fully removing, the temporal dependence of the remaining, i.e., "background," earthquakes [*van Stiphout et al.*, 2012]. We here use two distinct methods to decluster, so to evaluate which features of our analysis are robust with respect to the declustering approach.

The first method (M1) is a straightforward development of *Zhuang et al.* [2002, 2004], which is based on a space-time Epidemic-Type Aftershock Sequence (ETAS) model [*Ogata*, 1998]. The original method was designed to estimate a spatially nonuniform, but temporally constant, background rate. We here modify it to also explore the possible nonstationarity of the background seismicity, in order to detect long-term changes.

We model earthquake occurrences using the number of earthquakes per unit time and unit area $\lambda(x, y, t)$, defined as the sum of two contributions

$$\lambda(x, y, t) = \mu(x, y, t) + \nu(x, y, t) \tag{1}$$

in which ν accounts for triggering by previous earthquakes, and μ is the activity that would occur in the absence of any such interactions, i.e., the background rate. Triggering by previous earthquakes occurring at $\{x_i, y_i, t_i\}$ is modeled as

$$\nu(x, y, t) = \sum_{i/t_i<t} \frac{Ke^{\alpha m_i}}{(t + c - t_i)^p} \times \frac{\gamma - 1}{2\pi} \times \frac{L_i^{\gamma-1}}{\left((x - x_i)^2 + (y - y_i)^2 + L_i^2\right)^{\frac{\gamma+1}{2}}} \tag{2}$$

i.e., the product of the Omori-Utsu law with a power law spatial density. We define the characteristic length (or rupture radius) $L_i = 10^{0.5(m_i-2)}$ in kilometer [*Utsu and Seki*, 1955; *Van der Elst and Shaw*, 2015]. We fix the model parameters to $\alpha = 2$, $p = 1$ (since previous estimates of p performed for Japan using the JMA catalog range from $p \simeq 0.9$ [*Marsan et al.*, 2013] to $\simeq 1.1$ [*Zhuang et al.*, 2004]), $c = 10^{-3}$ days (sensitivity of our results on the c value is very weak for c in the 1 min ($\simeq 7\,10^{-4}$ days) to 1 h ($\simeq 0.04$ days) interval), and $\gamma = 2$ (consistent with $1.7 < \gamma < 2.1$ usually found for the decay of the linear density of aftershocks [cf. *Felzer and Brodsky*, 2006, *Marsan and Lengliné*, 2010]). Sensitivity to the choice of the α parameter value is discussed in the supporting information. Parameter K is a normalization coefficient that controls the total number of earthquakes, and it must therefore be estimated. The values of $\nu(x_i, y_i, t_i)/K$ are computed once and for all, making the rest of the computation fast, as described below.

The probability that i is a background earthquake is $\omega_i = \frac{\mu(x_i,y_i,t_i)}{\lambda(x_i,y_i,t_i)}$. We start by taking arbitrary (but nonzero) values of ω_i, e.g., $\omega_i = 0.5$, and smooth these values in space and time to obtain the a priori background rate:

$$\mu(x,y,t) = \sum_i \omega_i e^{-\sqrt{(x-x_i)^2+(y-y_i)^2}/\ell}\, e^{-|t-t_i|/\tau} \times \frac{1}{2\pi\ell^2 a_i} \tag{3}$$

where ℓ and τ are two smoothing parameters. In the following, we will investigate changes in background rate at the $\ell = 50$ km and $\tau = 1$ year scales. This choice of τ is dictated by the need to smooth out rapid, possibly nonrobust fluctuations, while capturing the slow trend that characterize the background rate. Other choices of τ in the 1 to 5 year interval give similar results. The dependence on ℓ is stronger: for example, a larger smoothing length of $\ell = 200$ km yields deceleration over the whole extent of the studied area, as the smoothing is then too strong given the size of the zones that display acceleration (see section 3). A $\ell \leq 100$ km is required to preserve those accelerating areas. Coefficients a_i are defined as $a_i = 2\tau - \tau\left(e^{-\frac{t_s-t_i}{\tau}} - e^{-\frac{t_e-t_i}{\tau}}\right)$ where t_s and t_e are the starting and ending time of the catalog, respectively (corresponding here to 1 January 1990 and 9 March 2011).

Parameter K is computed as

$$K = \frac{\sum_i 1 - \omega_i}{\sum_i F_i} \tag{4}$$

where $F_i = e^{\alpha m_i}\left(\ln(t_e + c - t_i) - \ln c\right)$ (for $p = 1$ as assumed here). This corresponds to the Maximum Likelihood Estimate of K. Knowing both μ and K, the a posteriori probabilities ω_i can then be computed, and the procedure is thus iterated until all values eventually converge to their final estimates. The latter do not depend on the initial, arbitrary choice of ω_i. Changes in background rates will be studied in section 3 by analyzing the temporal dependence of $\mu(x, y, t)$.

The first earthquake in the catalog is necessary a background earthquake, i.e., $\omega_1 = 1$, as there are no earthquakes in the analyzed data set that could explain its occurrence. Likewise, the background probabilities are overestimated for the first part of the catalog. As a result, a spurious slowing down with time of the background rate can be generated, which would interfere with our analysis of slow variations of background rate. We thus take care of this issue by using the $m \geq 3$ earthquakes in the 1 January 1980 to 31 December 1989 period as additional potential triggers for the targeted 1 January 1990 to 9 March 2011 period. These earthquakes are only used in the summation of equation (2), i.e., the sum $\sum_{i/t_i<t}$ is performed on all earthquakes i preceding time t, including 1980–1990 earthquakes. Including this 10 year long training period is effective in removing spurious decelerations: as shown in Figure S1 in the supporting information, it takes about 6 years of training to stabilize the background probabilities, so a 10 year long period can be considered sufficiently long for this purpose. We finally end up with $\sum_i \omega_i = 5591$ background earthquakes, hence about 34% of the total number.

The second method (M2) is based on the single-link clustering approach of *Zaliapin et al.* [2008]. The space-time distance $\eta_{ij} = T_{ij}R_{ij}$ between any two earthquakes $i < j$is computed, with $T_{ij} = (t_j - t_i)10^{-0.5bm_i}$ and $R_{ij} = \left\{(x_j - x_i)^2 + (y_j - y_i)^2\right\}^{d_f/2} 10^{-0.5bm_i}$. We here use the parameters $b = 0.8$ and $d_f = 1.52$, the reason for this choice being explained below. For earthquake j, we select i^* such that $\eta_{i^*j} = \max_i \eta_{ij}$ and isolate on the $\ln R_{i^*j}$ versus $\ln T_{i^*j}$ plot the mode that corresponds to a Poisson distribution, i.e., all earthquakes with $\eta_{i^*j} > \eta_c$. We take $\ln \eta_c = -3.5$, which corresponds to the clearest departure from the Poisson mode, see Figure S2. This yields 9792 background earthquakes, making up a 59% proportion. Here again, we use the 1980–1990

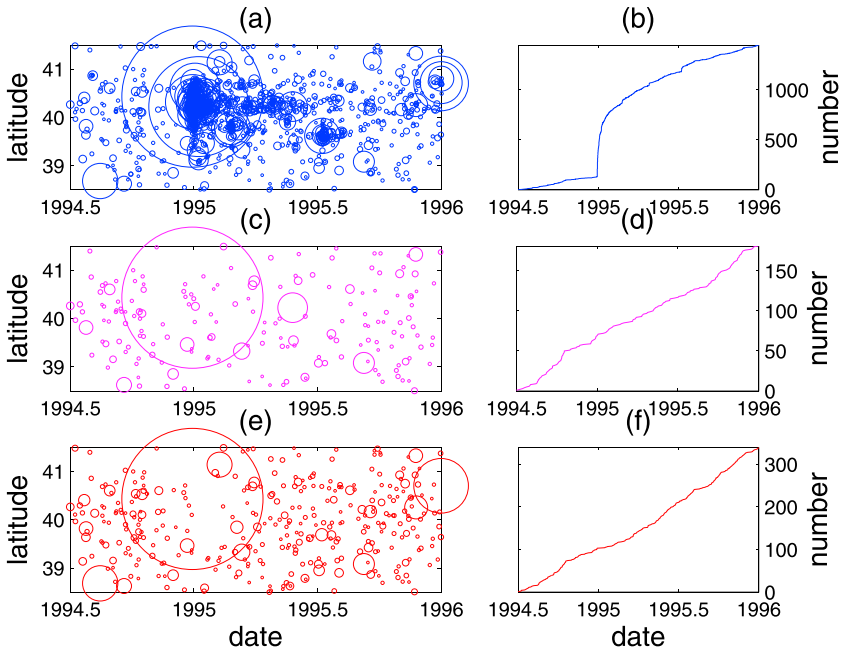

Figure 3. Example of a declustered sequence. (a and b) Space-time plot of the 1994 *M*7.6 Sanriku sequence and associated time series (see text for selection criteria for the earthquake data set). (c and d) Same as top graphs, for the catalog declustered with M1; we show a random realization of the declustered data set, given the background probabilities ω obtained by this method. (e and f) Same as top graphs, for the catalog declustered with M2.

earthquakes as potential triggers i^* to avoid contamination by edge effects. The selected 9792 earthquakes display a b value of 0.79 ± 0.01, and their epicenters define a set with fractal dimension $d_f = 1.52$, i.e., the correlation integral [*Grassberger and Procaccia*, 1983] $N(r)$ follows a power law $N(r) \sim r^{1.52}$ for 100m $< r <$ 100km, hence our choice of parameters b and d_f for computing T_{ij} and R_{ij}.

To illustrate how both methods behave, we show in Figure 3 the space-time plots of earthquakes, before and after declustering (with the two methods), zooming on the 1994 Sanriku sequence. For this example, and in order to facilitate the visual understanding of the map, the background earthquakes were selected for the first method by drawing uniform numbers between 0 and 1 and keeping only those for which this number is less than the background probability ω. It can be seen that both methods are efficient in removing aftershocks,

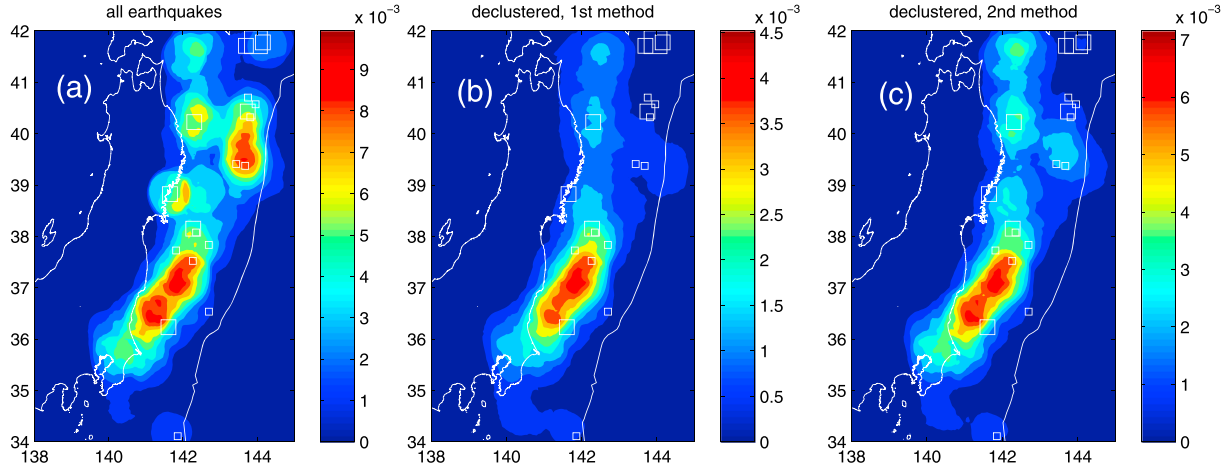

Figure 4. Earthquake density, $m \geq 3.0$, 1990–2011 period, smoothed over a length of 50 km, in number of earthquakes per year per square kilometer. (left) All earthquakes. (middle and right) After declustering, using either the first or second method, see text for details. The white squares are as in Figure 1. Notice the change in color scale between the two declustered maps.

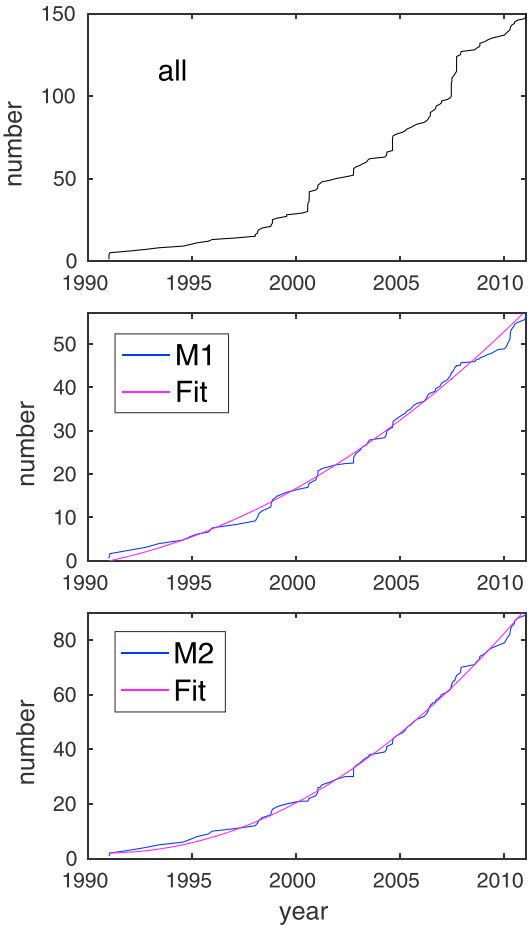

Figure 5. Example of time series for the node centered at 35° latitude and 141° longitude, offshore Boso. (top) All $m \geq 3$ earthquakes within 50 km of the node. (middle) Declustered time series according to method M1, in blue, with best quadratic fit, in magenta. The ratio of final to initial modeled rates gives $\phi_1 = 5.6$. (bottom) Same for method M2, giving $\phi_2 = 22.1$. In this case, both ϕ values are consistent (they both are >1).

leaving, respectively, 181 and 340 earthquakes out of the 1451 in the zone and time period. Since relatively little activity preceded the main shock, both methods find that it is a background earthquake, with M1 giving $\omega = 0.52$. We emphasize that this earthquake would not have been selected as a background earthquake, had foreshocks, even of small size (but still with $m \geq 3.0$), preceded it in its close vicinity.

Prior to the analysis of temporal fluctuations in the background rate, we map in Figure 4 the density of earthquakes, before and after declustering. Both declustering methods act to suppress the aftershock sequences of the 1992 and 1994 Sanriku earthquakes, leaving a low background density in the northern half of our area. In the southern half, similar to *Marsan et al.* [2013], we observe a robust, extended region of strong background activity, off the Fukushima and Ibaraki prefectures (approximately 36° to 38° of latitude), at depths of about 20 to 50 km. No large shocks have occurred in this zone in the studied period (1990–2011), explaining why the declustering marginally affects the seismicity. Magnitude 7 earthquakes are known to occur about every 20 years just south-east outside of this zone, the last occurrence taking place in 2008 [*Kubo et al.*, 2013], as indicated by the large white square in Figure 4. The southern limit of this zone corresponds to the northernmost extent of PHS [*Uchida et al.*, 2009]. This area mostly overlaps the cumulative rupture area of the 1938 sequence (cf. Figure 1), the last notable seismic crises to hit this place prior to 2011. *Abe* [1977] estimated from the lack of large earthquakes in historical records that the seismic coupling in this zone is about one tenth of the seismic coupling in neighboring areas. The 2011 *M*9.0 Tohoku earthquake and its *M*7.9 aftershock that occurred about 30 min later more to the south eventually broke this area. This gap between the two ruptures is potentially related to this frictional heterogeneity, further evidenced by the observation by *Koper et al.* [2011] that short-period radiations during the M9.0 rupture originate mostly from downdip and south of the hypocenter. Finally, very low earthquake density is observed near the Japan trench, especially in the south (around latitude 35°), although a regional high in background activity clearly delineates the Sagimi Trough.

3. Slow Changes in Background Activity

In order to investigate local changes in background rate, we use a grid with 0.05° spacing. For each node, we consider all the earthquakes within 50 km and discard the nodes with fewer than 50 earthquakes. For the remaining nodes, we compute the best quadratic fit $\hat{N}(t) = at^2 + bt + c$ to the cumulative time series of background earthquakes $N(t)$, with the additional constraint that the initial rate $2at_e + b$ and the final rate $2at_s + b$ must be positive. We then characterize the overall trend of this time series with the value

$$\phi = \frac{\dot{N}(t_e)}{\dot{N}(t_s)} = \frac{2at_e + b}{2at_s + b} \tag{5}$$

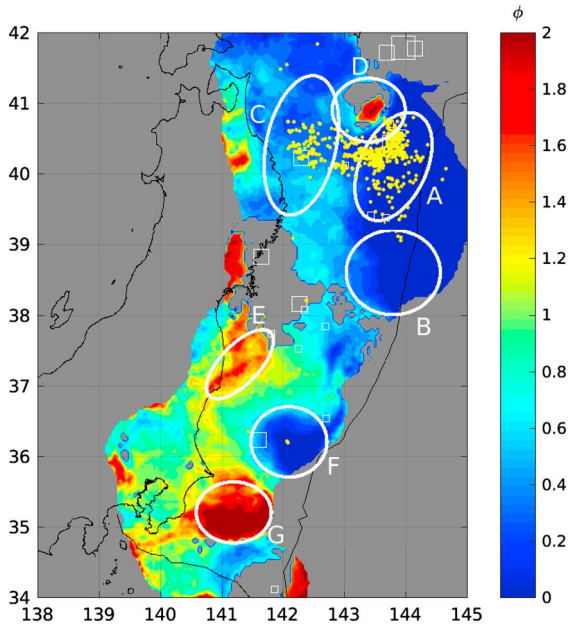

Figure 6. Map of acceleration/deceleration value ϕ. All earthquakes occurring within 10 days after the 28 December 1994 M_w7.6 Sanriku earthquake are shown in yellow. The white squares are as in Figure 1. Ellipses A–G are areas showing interesting features that receive specific attention, see Figure 7.

i.e., the ratio of the modeled final background rate by the modeled initial background rate. The two regimes of overall acceleration or deceleration are thus given by $\phi > 1$ and $\phi < 1$, respectively. We illustrate this in Figure 5 for a particular node offshore Boso.

We only keep the nodes that exhibit consistent ϕ values (ϕ_1, ϕ_2) for the two declustering methods, namely: either $\{\phi_1 > 1, \phi_2 > 1\}$ or $\{\phi_1 < 1, \phi_2 < 1\}$, or $|\phi_1 - \phi_2| < 0.3$. For those nodes, we finally compute and display $\phi = \frac{\phi_1+\phi_2}{2}$ in Figure 6; time series for the specific areas outlined in this map are given in Figure 7. We report in the supporting information how this consistency criterion constrains our results, as well as the sensitivity of our results on the α value used for the model of method M1 [*Felzer et al.*, 2004; *Hainzl et al.*, 2008, 2013; *Helmstetter et al.*, 2005; *Marsan et al.*, 2013; *Reverso et al.*, 2015; *Zhuang et al.*, 2004]. We now investigate in more details specific areas.

In the northern part of our study area (zones A, B, and C), deceleration starts at the end of 1997/beginning of 1998 with a rather abrupt decrease in rate, coincident with the termination of the afterslip of the 1994 M_w7.6 Sanriku earthquake [*Heki*, 2007]. Zooming on this main shock (zone A, which also includes the 1992 sequence [*Kawasaki et al.*, 2001]), the aftershock sequence is found to depart from the best Omori-Utsu law (with or without including a preseismic rate), see Figure S3, with too few observed aftershocks after about 1000 days as compared to these best fits, hence a rate anomalously low starting at 1997.9 and onward. We also modeled the $m \geq 5.0$ time series since 1960, as the superposition of a background constant (stationary) rate with Omori-Utsu laws initiated by the eight main shocks that most affected these time series. Here also, a relative quiescence follows the 1994 Sanriku earthquake, its start occurring between 1996 and 2000 (Figure S4). The seismicity dynamics of this zone is made complicated by the occurrence of several intermediate to large shocks; however, the fact that the two declustering methods, as well as the Omori-Utsu modeling of the 1994 M_w7.6 aftershock sequence and the modeling of the longer time series (since 1960), agree to point out a deficit in earthquake activity after at least 1998 makes this observation robust. A similar deficit with the same timing is also observed for zone C, which hosts the afterslip of the Sanriku earthquake [*Yagi et al.*, 2003] and some of its aftershocks (yellow dots in Figure 6), and also, and quite remarkably, for zone B, although this zone is off the rupture zone of this earthquake. Zone B overlaps with the large slip area of the 2011 M_w9.0 Tohoku earthquake, which, according to our analysis, experienced a slowing down of the background activity over 20 years preceding this event. A realization of the M1 declustered seismicity is plotted in Figure 8 in comparison with raw seismicity. The clear, spatially extended, quiescence can readily be spotted by eye from about 1998 at latitudes 38° to 42°.

In our selection, 1233 earthquakes have $z = 0$, most of them occurring in the 1990–1998 interval, and are mostly aftershocks of the 1992 and 1994 Sanriku sequences. Spurious trends in seismicity could result from an improved estimation of depth after 1998: near the trench, all $z = 0$ earthquakes are kept in our selected data set as they are within 20 km of the slab upper surface. As z is better estimated, previously found $z = 0$ values become fewer, implying that fewer earthquakes are counted near the slab, resulting in an apparent, spurious deceleration. We therefore checked whether the observed deceleration near the trench north of 38° of latitude could be caused by this issue. More specifically, we performed two analyses: (1) we increased the maximum distance to the slab for selecting earthquakes (from 20 km to 35 km, thus still avoiding keeping crustal earthquakes); (2) we attributed an approximated depth to all $z = 0$ earthquakes by taking the mean

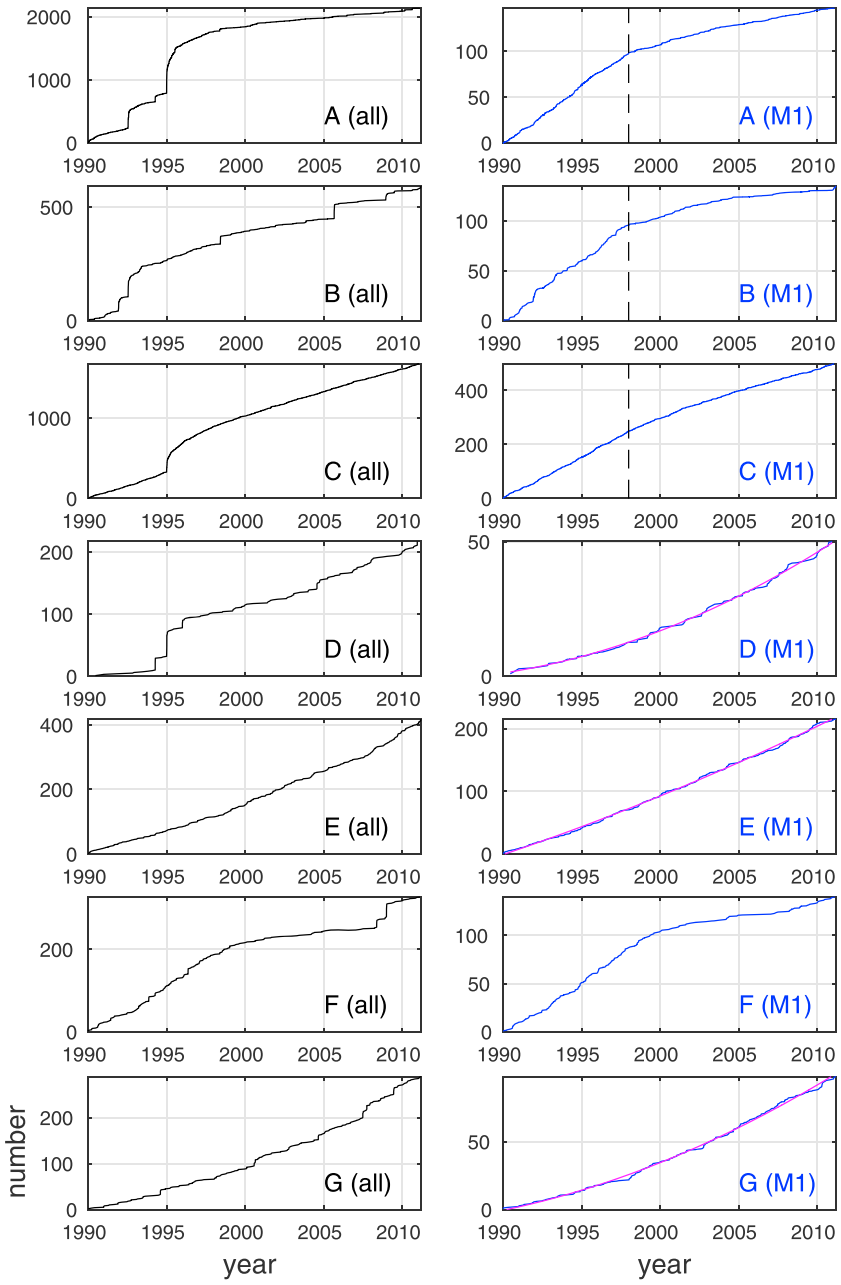

Figure 7. Earthquake activity in zones A to G, (left column) before and (right column) after declustering with method M1. The best quadratic fit to the declustered time series is shown in magenta for accelerating zones D, E, and G. The vertical line marks year 1998 for zones A, B, and C (after declustering). Very similar results are obtained with method M2.

depth of the 10 closest (in time) $z \neq 0$, $m \geq 3$ earthquakes with epicenter distance within 20 km. Those $z \neq 0$ earthquakes were not constrained to be close to the slab, i.e., we did not add any other requirement regarding their depths. In both cases, the resulting ϕ map is very similar (Figure 6). In particular, the observed deceleration in zones A, B, and C remains clearly an outstanding feature.

Engulfed in this 400 km large area of decelerating background activity, zone D displays a noticeable strong acceleration, see Figure 7. This acceleration is also evident in the raw rate time series. This zone is centered on the epicenter of the 1968 M_w8.3 Tokachi earthquake, a zone which experienced little coseismic slip, the two main asperities (i.e., large slip area) that broke lying downdip of the epicenter [*Nagai et al.*, 2001]. The time series of $m \geq 5.0$ earthquakes since 1923 shows that this zone entered a relative quiescence after 8 years of aftershock activity following the 1968 main shock, lasting at least until 1994, see Figure 9. This suggests

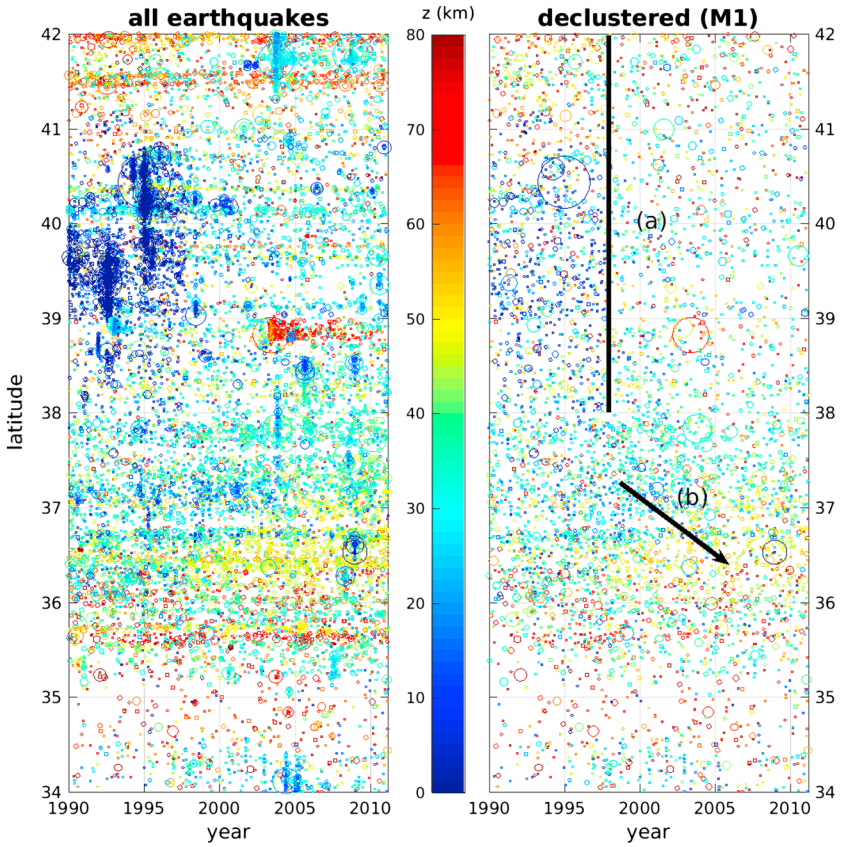

Figure 8. Space time plot of (left) all earthquakes and background earthquakes according to (right) method M1. Earthquakes are color-coded according to depth. In the declustered plot, a random realization given the background probabilities is shown. Large-scale patterns do not depend on the specific realization, i.e., they are statistically stable. A clear quiescence in the northern half is observed (a). An apparent migration from shallow to greater depths is evident at intermediate latitudes (b), coherent with the observed deceleration of zone F and acceleration of zone E (Figure 6). We observe the same features with method M2.

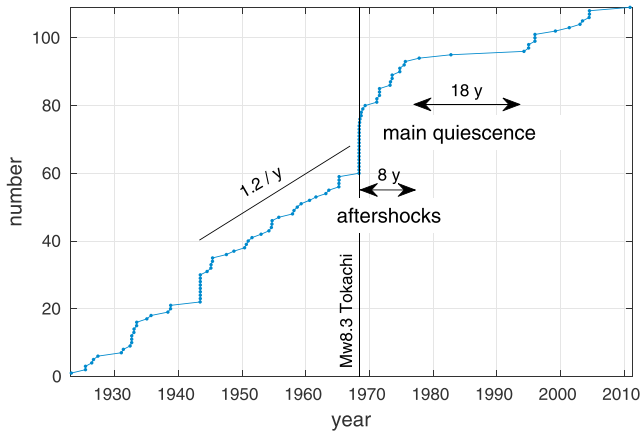

Figure 9. Time series of $m \geq 5.0$ earthquakes since 1923 for zone D, only using epicenter coordinates. The rate is stable at 1.2 per year for more than 25 years before the 1968 Tokachi earthquake. After 8 years of aftershock activity, the zone entered a quiescence still ongoing in 2011 (the rate being still lower than 1.2 per year), characterized by an 18 year long main phase of strongest rate decrease. The zone has been recovering from this quiescence since 1994–1995 and the occurrence of the Sanriku sequence.

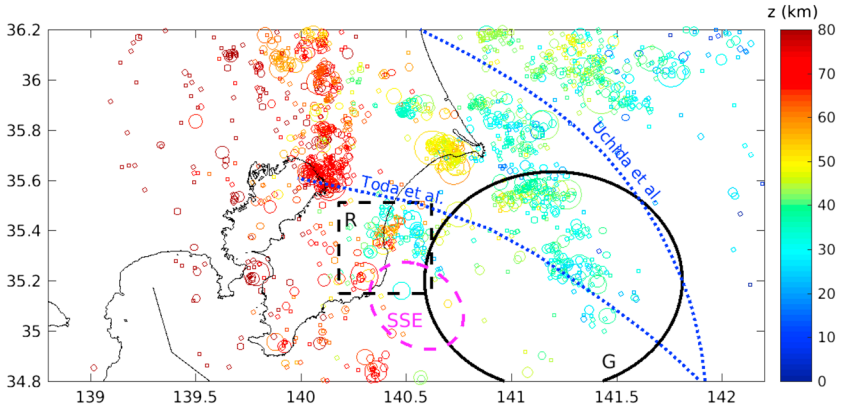

Figure 10. Map of earthquake activity close to zone G (black ellipse). The box (denoted R) studied by *Reverso et al.* [2016] is outlined with dashed lines. The location of slow slip for a typical Boso SSE is shown with the magenta dashed contour [*Ozawa*, 2014]. Contours of the northernmost limit of the Philippine Sea plate are shown, according to *Uchida et al.* [2009] and *Toda et al.* [2008].

that the observed acceleration of background activity in 1990–2011 results from a slow recovery after an 18 year long phase of strong quiescence, during which only 2 $m \geq 5.0$ earthquakes occurred, compared to the average 21 earthquakes as expected for a 1.2 per year rate.

In the southern half of the studied area, strong acceleration is found far offshore Kanto (zone G of Figure 6). The clusters of earthquakes that exhibit an accelerated rate of occurrence over 1990–2011 are located about halfway between the coast of Kanto and the Japan trench, at depths of about 20 km for the easternmost sources to about 50 km, cf. Figure 10. These depths are coherent with earthquake activity related to PAC [*Ishida*, 1992; *Hayes et al.*, 2012], although the proximity to the Sagimi Trough suggests that the PHS subduction could also contribute. Indeed, in this area, PHS is expected to be in contact with PAC [*Uchida et al.*, 2009], although a different interpretation, based on a change in the plate motion direction 5 M year ago, exists [*Toda et al.*, 2008]. Direct inspection of cross sections shows no apparent dip toward north; moreover, 1997–2016 F-NET focal mechanisms for thrust (i.e., 70°<rake< 110°) earthquakes with dip < 20° give a mean strike of 191° in this zone, which agrees with slip on either the PAC-PHS or PAC-OKH interfaces [*Uchida et al.*, 2009]. This leads us to conclude that the earthquakes selected in this zone are effectively caused by the displacement of PAC relative to both OKH and PHS.

Zones E and F show opposite behaviors, with deceleration at shallow depth (zone F) contrasting with acceleration downdip (zone E). This pattern can be also seen in Figure 8, with an apparent, long-term migration of activity at latitudes 36° to 38° from shallow to greater depths. Zone F encompasses subducting seamounts that could locally reduces the coupling [*Mochizuki et al.*, 2008].

4. Discussion

4.1. Relationship With Seismic Coupling

The background earthquake rate that we image corresponds to the part of seismic activity after removing aftershocks. It is seen as a proxy to tectonic forcing, i.e., convergence rate in the context of subduction [*Bird et al.*, 2009; *Ide*, 2013]. Changes in background rate over a timescale of 21 years cannot, however, be attributed to equivalent changes in convergence rate, given both (i) the very short timescales implied relative to those involved in the drift of Euler poles or changes in plate displacement rates, and (ii) the large amplitude of the changes we observe. For example, accelerations in zones D and G are characterized by $\phi = 4.14$ and $\phi = 3.77$, respectively (cf. Figure 7). Positive and negative changes in seismic coupling are known to exist in the Japanese subduction at the 10 year timescale [*Mavrommatis et al.*, 2014; *Yokota and Koketsu*, 2015; *Loveless and Meade*, 2016]. Progressive decoupling of the plate interface implies accelerated slip on the subduction interface, hence accelerated seismicity, as for example observed during Boso slow slip events [*Ozawa*, 2003; *Ozawa et al.*, 2007; *Hirose et al.*, 2014]. Transient increase in local slip rate has indeed been suggested as the driving mechanism for aftershock triggering [*Perfettini and Avouac*, 2004], and swarm activity [*Ozawa et al.*, 2007], in each case the seismic moment relaxed by earthquakes being only a very small part—typically amounting to a few percents—of the total seismic moment relaxed by slow slip.

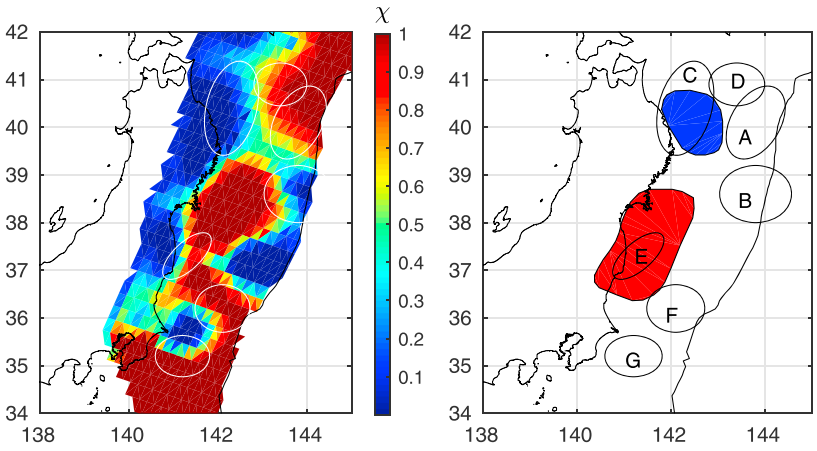

Figure 11. Maps showing (left) the 1997–2000 interseismic coupling of *Cubas et al.* [2015] and (right) the location of the areas experiencing increased (in red) and decreased (in blue) slip rate, according to the inversion of *Yokota and Koketsu* [2015], which is similar to the inversion of *Mavrommatis et al.* [2014].

We therefore attribute the observed changes in background rates to changes in seismic coupling: background seismicity is merely a passive marker of local slip rate, excluding coseismic slip and afterslip. Denoting seismic coupling by χ, the aseismic slip rate is $(1-\chi)\dot{\delta}_0$, with $\dot{\delta}_0$ the local convergence rate. This aseismic slip with rate equal to $(1-\chi)\dot{\delta}_0$ gives birth to seismicity with background rate μ, depending on the local density of velocity-weakening patches (i.e., asperities). The relationship between $(1-\chi)\dot{\delta}_0$ and μ is likely a complex issue, in particular depending on the distribution of asperity sizes and their spatial distribution over the area [*Dublanchet et al.*, 2013]. Assuming that the proportionality between these two quantities is locally constant over time, and that $\dot{\delta}_0$ does not vary either over 21 years, the relative change in aseismic slip rate $\frac{1-\chi_2}{1-\chi_1}$ equals $\phi = \frac{\mu_2}{\mu_1}$, with χ_1 the initial and χ_2 the final coupling coefficients, and μ_1 and μ_2 the initial and final background rates.

It is likely that a similar proportionality exists between the total slip rate (i.e., including coseismic slip and afterslip of large main shocks) and the total earthquake rate (i.e., including aftershocks), controlled by thermal and structural properties that can be considered constant at the timescale of tens of years. However, both these total rates are strongly dependent on the presence or not of large main shocks during the limited observation period, giving birth to severe sampling issues that would hide genuine trends affecting both rates at the observation timescale. The use of aseismic slip and background seismicity rates is only intended to address this sampling issue, by reducing as much as possible the direct influence of the largest main shocks.

4.2. Comparison With Changes in Coupling as Observed by GPS

Our observations are in agreement with those of *Mavrommatis et al.* [2014] and *Yokota and Koketsu* [2015], cf. Figure 11b. The inverted 2003–2011 decoupling downdip of the *M*9.0 epicenter, from about 36.5° to 38.5° in latitude, correlates with our zone E, while the strengthening of coupling at 39.5° to 40.5° overlaps with our zone C. However, the changes in coupling observed by GPS miss large parts of our observed changes in background seismicity. We can think of two explanations for this apparent discrepancy.

1. Equivalent seismicity changes lead to stronger changes in GPS displacement rates—both for positive and negative changes—for zones that are less coupled. Keeping with our previous notations, and assuming the simplest model $\phi = \frac{1-\chi_2}{1-\chi_1}$ is valid, we get that the change in coupling is $\Delta\chi = \chi_2 - \chi_1 = (1-\chi_1)\times(1-\phi)$. GPS inversions are sensitive to the change in coupling $\Delta\chi$, at constant plate convergence rate. A lower χ_1 will thus cause a larger $|\Delta\chi|$, at constant ϕ, whatever the sign of ϕ. In the northern and southern halves of our studied area, among observed significant changes ϕ in background rates, the less coupled areas according to *Cubas et al.* [2015] are zones C and E, respectively (Figure 11a), which effectively correspond to where GPS inversions locate the dominant changes in coupling.
2. The sensitivity of GPS measurements to slip decays with distance, gradually reducing the capacity of GPS inversions to robustly image coupling far offshore. The zones closest to inland stations are thus

best resolved. This could explain why zone B, which background rate significantly decelerates and is characterized by low coupling, does not exhibit geodetically resolvable changes in coupling.

Since coupling is only moderate at the level of the Honshu coastline, these two effects reinforce one another.

Time series of repeating earthquakes have been studied by *Uchida and Matsuzawa* [2013], thereinafter referred to as UM, for the 1985–2011 period, thus largely overlapping our target period. The effect of major local earthquakes is, however, clearly visible in most of these time series and should be removed in order to check whether background rates of repeaters have evolved or not. Among the zones where repeaters occur and are visually not significantly affected by local strong earthquakes, only two are well resolved by our analyses: zone 4 of UM shows deceleration and is located in our zone C, while zone 12 of UM shows acceleration and is located in our zone E. In both cases, the patterns are consistent between the two studies.

The same is also true for the repeating earthquake analysis of *Mavrommatis et al.* [2015], apart from zone F, which they found to be accelerating for the 1996–2011 period they targeted. This apparent acceleration could be caused by the occurrence of the 2008 *M*7.0 Ibaraki earthquake, which epicenter is located in zone F. Time series of repeating earthquakes 1165 and 1411 of their Figure 2 show that the last two occurrences (out of four) happened after this main shock, the first of these two occurrences even immediately after. *Mavrommatis et al.* [2015] attempted to correct for afterslip of $M_w \geq 6.3$ main shocks using the model of *Johnson et al.* [2013]. In the light of their Figure 2, we argue that this correction, at least for groups 1165 and 1411, is underestimated. The seismicity in zone F is clearly sensitive to the 2008 main shock; declustering is required to remove this sensitivity, cf. Figure 6.

Our observations globally point to a strengthening of coupling after 1998 updip of the megathrust, and more localized weakening of coupling at greater depths (below 40 km). Both processes act to increase the loading shear rate of the more coupled portion of the megathrust, which eventually ruptured during the 2011 Tohoku earthquake. While we cannot evaluate whether this pattern could be a premonitory sign of the impending rupture, in any case it did clock advanced the occurrence of the main shock.

4.3. Regional Acceleration Along the Sagimi Trough

We observe in zone G a continuous acceleration of background seismicity, strikingly similar to the one already reported in *Reverso et al.* [2016] for the Boso area, 1990–2015. In both cases, the declustered time series is well modeled by a quadratic fit, i.e., a constant acceleration over 21 or 25 years. Zone G shows extremely marginal overlap with the area (denoted R from there on) analyzed by *Reverso et al.* [2016], cf. Figure 10, so this observation is new. Moreover, repeating earthquakes in R exhibit the same type of constantly accelerating time series, when removing swarms due to slow slip events, for the 2004–2015 period, but only for PHS. Repeating earthquakes on PAC display a distinct trend, characterized by a constant rate of occurrence up to the time of the 2011 *M*9.0 Tohoku earthquake, followed by postseismic increase and relaxation afterward, with no apparent long-term acceleration.

The increase in stressing rate of the SSE patch cannot be directly observed, given the absence of seismicity on the patch. However, shortening of the waiting time between successive SSE has been documented by *Ozawa* [2014] and linked to the acceleration of seismicity in R by *Reverso et al.* [2016].

In zone G, focal mechanisms of gently dipping thrust repeating earthquakes are consistent with slip along an interface between PHS and PAC, so that the two plates are in contact there [*Uchida et al.*, 2009]. Mechanical coupling between zones G, R, and the patch hosting SSEs is therefore expected. This is further suggested by the observation that zone G hosted very brief bursts of activity weeks before and after the 2007 M_w6.6 SSE [*Ozawa et al.*, 2007] in Boso, see Figure S5; in particular, about 2 months prior to the SSE, a $m = 5.0$ followed by three $m = 4.5$ to 4.8 events occurred within 5 h of each other. The rapid succession of four earthquakes with comparable sizes is a typical signature of swarm activity, possibly triggered by aseismic slip.

Accelerated activity over 20+ years in zones G, R, and the SSE patch hints at a regional process acting along a > 100 km long stretch of the Sagimi Trough, which amounts to a weakening of seismic coupling between PHS and PAC, and PHS and OKH, although it seems difficult to envision a process that could equally spread on two plate interfaces at different depths. *Nishimura et al.* [2007] found a very low coupling between PAC and PHS (their zone D), although it is badly resolved. For a significant increase in aseismic slip to occur, the initial coupling cannot be too small. We therefore expect that coupling between PHS and PAC is at least intermediate

in zone G and has been decreasing from 1990 to 2011. This would extend more to the north the local high in PAC-PHS coupling located at about 141° of longitude by *Noda et al.* [2013].

4.4. Unexplained Features

The observed slowing down in background rate in zones A, B, and C after 1998 appears related to the termination of the postseismic slip following the 1994 Sanriku earthquake. Zone B is located away from this rupture, cf Figure 6 and the 10 day aftershocks of this sequence (yellow dots), and did not host any afterslip according to *Yagi et al.* [2003]. It is unclear why this quiescence extends over such a large area.

The acceleration in zone D appears spatially limited to a 50×50 km^2 area, although it could possibly extend farther to the north in the rupture zone of the 2003 Tokachi earthquake, this zone being unresolved for background seismicity dynamics. Our analysis suggests that zone D has been in the process of recovering from quiescence following the 1968 Tokachi earthquake, during the 1990–2011 period. Compared to postseismic quiescences observed in California [e.g., *Ellsworth et al.*, 1981], the recovery time is here relatively short (18 years compared to 50 years for the 1906 San Francisco earthquake), possibly owing to a higher stressing rate and differences in stress drop. The question remains as to why the 1990–2011 acceleration only affects such a limited area, rather than the whole of the 1968 rupture zone, especially as zone D is not located on the main slip areas of the 1968 main shock (we however note that maximum bending of the subducting plate occurs there, so that it could effectively correspond to an asperity, as proposed by *Ito et al.* [2004]). In comparison, at the time of the 1994 M_w7.6 Sanriku earthquake, the southern 1968 asperity had already fully recovered since it reruptured then. While we cannot give any satisfactory explanation for the limited size of zone D and its peculiar behavior in the wake of the 1968 main shock, this at least demonstrates that healing/recoupling can be spatially very heterogeneous in this context.

5. Conclusions

We analyzed the 1990–2011 evolution of background seismicity, i.e., earthquake rate after removing aftershocks, for the northern Japanese subduction zone (latitude 34° to 42°), using two independent declustering methods in order to isolate the most robust features. Significant changes are observed, with final to initial rate ratio as high/low as ×4 or ×1/4. More specifically, a decrease in activity for most of the northern half (38° to 42° of latitude), with a clear change point at about 1998, is the strongest signal we found. This, and the spatially localized acceleration in zone D, can be explained by post–main shock quiescence and further recovery from it. We emphasize that recovery can be relatively fast compared to other plate boundaries with a fully locked schizosphere, likely owing to the fact that coupling is not 100% over the velocity-weakening slice of the slab. Moreover, sharp spatial contrasts in recovery time are observed (i.e., zone D).

Accelerated seismicity offshore Kanto is a robust trend, which strengthens previous observations, all pointing to a regional decoupling process along a 100 km long stretch of the Sagimi Trough. Repeating earthquakes on PHS show a similar acceleration, up to 2015, hence well past the 2011 Tohoku earthquake; this decoupling is therefore quite possibly not over by now (2016). How this pattern will evolve in the future is not predictable, since such a long-term trend, not related to post–main shock quiescence like in the north, has not been observed elsewhere.

Acknowledgments

The JMA unified catalog used in this study is produced by the Japanese Meteorological Agency, in cooperation with the Ministry of Education, Culture, Sports, Science and Technology. This unified catalog is available at the JMA website www.jma.go.jp/jma/indexe.html. We would like to thank two anonymous reviewers and the Associate Editor for their help in improving this manuscript.

References

Abe, K. (1977), Tectonic implications of the large Shioya-oki earthquakes of 1938, *Tectonophysics*, *41*, 269–289.

Bird, P., Y. Y. Kagan, D. D. Jackson, F. P. Schoenberg, and M. J. Werner (2009), Linear and nonlinear relations between relative plate velocity and seismicity, *Bull. Seismol. Soc. Am.*, *99*, 3097–3113.

Cubas, N., N. Lapusta, J. P. Avouac, and H. Perfettini (2015), Numerical modeling of long-term earthquake sequences on the NE Japan megathrust: Comparison with observations and implications for fault friction, *Earth Planet. Sci. Lett.*, *419*, 187–198.

Dublanchet, P., P. Bernard, and P. Favreau (2013), Interactions and triggering in a 3-D rate-and-state asperity model, *J. Geophys. Res. Solid Earth*, *118*, 2225–2245, doi:10.1002/jgrb.50187.

Ellsworth, W. L., A. G. Lindh, W. H. Prescott, and D. G. Hedr (1981), The 1906 San Francisco earthquake and the seismic cycle, in *Earthquake Prediction: An International Review*, edited by D. W. Simpson and and P. G. Richards, AGU, Washington, D. C.

Felzer, K. R., R. E. Abercrombie, and G. Ekstrom (2004), A common origin for aftershocks, foreshocks, and multiplets, *Bull. Seismol. Soc. Am.*, *94*, 88–98.

Felzer, K. R., and E. E. Brodsky (2006), Decay of aftershock density with distance indicates triggering by dynamic stress, *Nature*, *441*, 735–738.

Grassberger, P., and I. Procaccia (1983), Characterization of strange attractors, *Phys. Rev. Lett.*, *50*, 346–349.

Hainzl, S., A. M. Christophersen, and B. Enescu (2008), Impact of earthquake rupture extensions on parameter estimations of point-process models, *Bull. Seismol. Soc. Am.*, *98*, 2066–2072.

Hainzl, S., O. Zakharova, and D. Marsan (2013), Impact of aseismic transients on the estimation of aftershock productivity parameters, *Bull. Seismol. Soc. Am.*, *103*, 1723–1732.
Hayes, G., D. J. Wald, and R. L. Johnson (2012), Slab1.0: A three-dimensional model of global subduction zone geometries, *J. Geophys. Res.*, *117*, B01302, doi:10.1029/2011JB008524.
Heki, K. (2007), Secular, transient, and seasonal crustal movements in Japan from a dense GPS array, in *The seismogenic zone of subduction thrust faults*, edited by T. Dixon and and C. Moore, Columbia Univ. Press, 512–539.
Heki, K., and Y. Mitsui (2013), Accelerated Pacific plate subduction following interplate thrust earthquakes at the Japan trench, *Earth Plan. Sci. Lett.*, *363*, 44–49.
Helmstetter, A. (2003), Is earthquake triggering driven by small earthquakes?, *Phys. Rev. Lett.*, *91*, 58501.
Helmstetter A., Y. Y. Kagan, and D. D. Jackson (2005), Importance of small earthquakes for stress transfers and earthquake triggering, *J. Geophys. Res.*, *110*, B05S08, doi:10.1029/2004JB003286.
Hirose, H., T. Matsuzawa, T. Kimura, and H. Kimura (2014), The Boso slow slip events in 2007 and 2011 as a driving process for the accompanying earthquake swarm, *Geophys. Res. Lett.*, *41*, 2778–2785, doi:10.1002/2014GL059791.
Ide, S. (2013), The proportionality between relative plate velocity and seismicity in subduction zones, *Nat. Geosci.*, *6*, 780–784.
Ishida, M. (1992), Geometry and relative motion of the Philippine Sea Plate and Pacific Plate beneath the Kanto-Tokai District, Japan, *97*, 489–513.
Ito, A., G. Fujie, T. Tsuru, S. Kodaira, A. Nakanishi, and Y. Kaneda (2004), Fault plane geometry in the source region of the 1994 Sanriku-oki earthquake, *Earth. Plant. Sci. Lett.*, *223*, 163–175.
Johnson, K. M., A. P. Mavrommatis, and P. Segall (2013), Small interseismic asperities and widespread aseismic creep on the northern Japan subduction interface, *Geophys. Res. Lett.*, *43*, 135–143, doi:10.1002/2015GL066707.
Kawasaki, I., Y. Asai, and Y. Tamura (2001), Space-time distribution of interplate moment release including slow earthquakes and the seismo-geodetic coupling in the Sanriku-oki region along the Japan trench, *Tectonophysics*, *330*, 267–283.
Koper, K. D., A. R. Hutko, T. Lay, C. J. Ammon, and H. Kanamori (2011), Frequency-dependent rupture process of the 2011 M_w9.0 Tohoku earthquake: Comparison of short-period *P* wave backprojection images and broadband seismic rupture models, *Earth Planet. Space*, *63*, 599–602.
Kubo, H., K. Asano, and T. Iwata (2013), Source-rupture process of the 2011 Ibaraki-oki, Japan, earthquake (M_w7.9) estimated from the joint inversion of strong-motion and GPS data: Relationship with seamount and Philippine Sea plate, *Geophys. Res. Lett.*, *40*, 3003–3007, doi:10.1002/grl.50558.
Loveless, J. P., and B. J. Meade (2016), Two decades of spatiotemporal variations in subduction zone coupling offshore Japan, *Earth Plan. Sci. Lett.*, *436*, 19–30.
Marsan, D. (2005), The role of small earthquakes in redistributing crustal elastic stress, *Geophys. J. Int.*, *163*, 141–151.
Marsan, D., and O. Lengliné (2010), A new estimation of the decay of aftershock density with distance to the mainshock, *J. Geophys. Res.*, *115*, B09302, doi:10.1029/2009JB007119.
Marsan, D., T. Reverso, A. Helmstetter, and B. Enescu (2013), Slow slip and aseismic deformation episodes associated with the subducting Pacific plate offshore Japan, revealed by changes in seismicity, *J. Geophys. Res. Solid Earth*, *118*, 4900–4909, doi:10.1002/jgrb.50323.
Matsuzawa, T., H. Hirose, B. Shibazaki, and K. Obara (2010), Modeling short- and long-term slow slip events in the seismic cycles of large subduction earthquakes, *J. Geophys. Res.*, *115*, B12301, doi:10.1029/2010JB007566.
Mavrommatis, A. P., P. Segall, and K. M. Johnson (2014), A decadal-scale deformation transient prior to the 2011 M_w9.0 Tohoku-oki earthquake, *Geophys. Res. Lett.*, *41*, 4486–4494, doi:10.1002/2014GL060139.
Mavrommatis, A. P., P. Segall, N. Uchida, and K. M. Johnson (2015), Long-term acceleration of aseismic slip preceding the M_w 9 Tohoku-oki earthquake: Constraints from repeating earthquakes, *Geophys. Res. Lett.*, *42*, 9717–9725, doi:10.1002/2015GL066069.
Mitsui, Y. (2015), Interval modulation of recurrent slow slip events by two types of earthquake loading, *Earth Planet. Space*, *67*, 1–8.
Mochizuki, K., T. Yamada, M. Shinohara, Y. Yamanaka, and T. Kanazawa (2008), Weak interplate coupling by seamounts and repeating *M*7 earthquakes, *Science*, *321*, 1194–1197.
Nagai, R., M. Kikuchi, and Y. Yamanaka (2001), Comparative study on the source process of recurrent large earthquakes in Sanriku-oki region: The 1968 Tokachi-oki earthquake and the 1994 Sanriku-oki earthquake, *Zisin*, *54*, 267–280.
Nishimura, T., T. Sagiya, and R. S. Stein (2007), Crustal block kinematics and seismic potential of the northernmost Philippine Sea plate and Izu microplate, central Japan, inferred from GPS and leveling data, *J. Geophys. Res.*, *112*, B05414, doi:10.1029/2005JB004102.
Noda, A., C. Hashimoto, Y. Fukahata, and M. Matsu'ura (2013), Interseismic GPS strain data inversion to estimate slip-deficit rates at plate interfaces: Application to the Kanto region, central Japan, *Geophys. J. Int.*, *193*, 61–77.
Okada, T., and A. Hasegawa (2003), The *M*7.1 May 26, 2003 off-shore Miyagi Prefecture earthquake in northeast Japan: Source process and aftershock distribution of an intra-slab event, *Earth Planet. Space*, *55*, 731–739.
Ogata, Y. (1998), Space-time point-process models for earthquake occurrences, *Ann. Inst. Stat. Math.*, *50*, 379–402.
Ozawa, S. (2003), Characteristic silent earthquakes in the eastern part of the Boso Peninsula, Central Japan, *Geophys. Res. Lett.*, *30*, 1283, doi:10.1029/2002gl016665.
Ozawa, S. (2014), Shortening of recurrence interval of Boso slow slip events in Japan, *Geophys. Res. Lett.*, *41*, 2762–2768, doi:10.1002/2014GL060072.
Ozawa, S., H. Suito, and M. Tobita (2007), Occurrence of quasi-periodic slow-slip off the east coast of the Boso Peninsula, Central Japan, *Earth Planet. Space*, *59*, 1241–1245.
Perfettini, H., and J. P. Avouac (2004), Postseismic relaxation driven by brittle creep: A possible mechanism to reconcile geodetic measurements and the decay rate of aftershocks, application to the Chi-Chi earthquake, Taiwan, *J. Geophys. Res.*, *109*, B02304, doi:10.1002/2014GL060072.
Reverso, T., D. Marsan, and A. Helmstetter (2015), Detection and characterization of transient forcing episodes, affecting earthquake activity in the Aleutian Arc system, *Earth Planet. Sci. Lett.*, *412*, 25–34.
Reverso, T., D. Marsan, A. Helmstetter, and B. Enescu (2016), Background seismicity in Boso Peninsula, Japan: Long-term acceleration, and relationship with slow slip events, *Geophys. Res. Lett.*, *43*, 5671–5679, doi:10.1002/2016GL068524.
Toda, S., R. S. Stein, S. H. Kirby, and S. B. Bozkurt (2008), A slab fragment wedged under Tokyo and its tectonic and seismic implications, *Nat. Geosci.*, *1*, 771–776, doi:10.1038/ngeo318.
Tormann, T., B. Enescu, J. Woessner, and S. Wiemer (2015), Randomness of megathrust earthquakes implied by rapid stress recovery after the Japan earthquake, *Nat. Geosci.*, *8*, 152–158.
Uchida, N., and T. Matsuzawa (2013), Pre- and postseismic slow slip surrounding the 2011 Tohoku-oki earthquake rupture, *Earth Planet. Sci. Lett.*, *374*, 81–91, doi:10.1016/j.epsl.2013.05.021.

Uchida, N., J. Nakajima, A. Hasegawa, and T. Matsuzawa (2009), What controls interplate coupling?: Evidence for abrupt change in coupling across a border between two overlying plates in the NE Japan subduction zone, *Earth Planet. Sci. Lett.*, *283*, 111–121.

Utsu, T., and A. Seki (1955), Relation between the area of aftershock region and the energy of the mainshock, *Zisin*, *7*, 233–240.

Van der Elst, N. J., and B. E. Shaw (2015), Larger aftershocks happen farther away: Nonseparability of magnitude and spatial distributions of aftershocks, *Geophys. Res. Lett.*, *42*, 5771–5778, doi:10.1002/2015GL064734.

van Stiphout, T., J. Zhuang, and D. Marsan (2012), Seismicity declustering, Community Online Resource for Statistical Seismicity Analysis, doi:10.5078/corssa-52382934. [Available at http://www.corssa.org/.]

Yagi, Y., M. Kikuchi, and T. Nishimura (2003), Co-seismic slip, post-seismic slip, and largest aftershock associated with the 1994 Sanriku-Haruka-Oki, Japan, earthquake, *Geophys. Res. Lett.*, *30*, 2177, doi:10.1029/2003GL018189.

Yokota, Y., and K. Koketsu (2015), A very long-term transient event preceding the 2011 Tohoku earthquake, *Nat. Commun.*, *6*, 5934, doi:10.1038/ncomms6934.

Zaliapin, I., A. Gabrielov, V. Keilis-Borok, and H. Wong (2008), Clustering analysis of seismicity and aftershock identification, *Phys. Rev. Lett.*, *101*, 18501.

Zhuang, J., Y. Ogata, and D. Vere-Jones (2002), Stochastic declustering of space-time earthquake occurrences, *J. Am. Stat. Assoc.*, *97*, 369–380.

Zhuang, J., Y. Ogata, and D. Vere-Jones (2004), Analyzing earthquake clustering features by using stochastic reconstruction, *J. Geophys. Res.*, *109*, B05301, doi:10.1029/2003JB002879.